Deformation mechanism of capsule-type hydrogen-storage-alloy actuator

Kenta Goto[a, *, 1], Tomoyuki Hirata[a], Takehiro Higuchi[b], Ohmi Fuchiwaki[c], Shingo Ozaki[c], Wataru Nakao[c]

a Graduate School of Engineering, Yokohama National University, 79-5 Tokiwadai, Hogaya, Yokohama 240-8501, Japan

b Faculty of Environment and Information Sciences, Yokohama National University, 79-5 Tokiwadai, Hogaya, Yokohama 240-8501, Japan

c Faculty of Engineering, Yokohama National University, 79-5 Tokiwadai, Hogaya, Yokohama 240-8501, Japan

* Corresponding author. E-mail: goto-kenta-wz@ynu.jp, Tel: +81-45-339-3692

Abstract

A capsule-type actuator using hydrogen storage alloy (HSA) was fabricated and its response behavior was investigated by experiment and finite element analysis. The capsule-type HSA actuator consists of an HSA foil placed on the inner wall of a capsule. In this paper, the displacement change of the actuator made of palladium foil and epoxy resin was experimentally measured in hydrogen atmosphere. As a result, it displaced with the decrease in the capsule height when hydrogen gas was charged, and vice versa. Displacement amount and response time of the actuator depended on the hydrogen pressure during the pressurization, while the response time was independent of the pressure during the evacuation. Also, the HSA actuator's deformation with hydrogen

[1] Research Center for Structural Materials, National Institute for Materials Science, 1-2-1 Sengen, Tsukuba 305-0047, Japan.

diffusion was simulated using the finite element method. It revealed that hydrogen content in the HSA foil was decreased by high compressive stress, indicating the hydrogen atom was absorbed as a solid solution phase in the HSA foil even when a surrounding hydrogen pressure was higher than the phase transition pressure.

Keywords

metal hydride; stress induced diffusion; finite element method; structural-diffusion coupled analysis; palladium

1. Introduction

A hydrogen-storage-alloy (HSA) actuator is an actuator using volume change of hydrogen storage alloy which reversibly absorbs hydrogen and expands with an increase in its surrounding H_2 pressure. The actuator is driven by the change in H_2 pressure and anticipated to be used in a hydrogen society that uses hydrogen as a major source of power [1, 2].

Two types of the HSA actuators have been developed, i.e. a unimorph-type actuator [3-10] and a capsule-type actuator [11, 12]. In the unimorph actuator, an HSA foil is bonded with a substrate. Expansion of the HSA foil in H_2 causes bending and twisting motion. Nishi et al. [3], for example, fabricated a unimorph actuator consisting of a $LaNi_5$ foil and a polyimide substrate for medical application. It showed a bending strain of ~0.1% under hydrogen of 0.12 MPa, and its shape recovered after the evacuation.

The capsule-type actuator [11, 12] was proposed for a super multi-link space manipulator to capture space debris [13]. The manipulator has multiple joints with the actuators to realize the flexible grasping. Another possible application is a smart regulator mounted on a fuel-cell vehicle, in which the flux of hydrogen is automatically controlled

45 depending on the pressure. In these structural applications, an actuator is required to have
46 high stiffness and lightweight in addition to good energy efficiency.
47 The capsule-type actuator has an axisymmetric structure consisting of a hollow capsule
48 and an HSA foil which is partially placed on the inner wall of the capsule (Figure 1),
49 which realizes high stiffness and lightweight. The HSA foil expands when H_2 gas is
50 charged into the capsule, causing the deformation of the capsule. The height change of
51 the capsule is used as an actuator's displacement. Goto et al. [11] estimated its static
52 performance by a finite element method (FEM) assuming that the HSA foil isotropically
53 absorbs hydrogen. They showed the capsule height decreases when the foil absorbs
54 hydrogen (Figure 1). This concept was experimentally confirmed with a capsule-type
55 actuator made of palladium and ABS resin [12]. The displacement was, however, much
56 smaller than that expected from the FEM simulation.
57 The performance of the HSA actuator is strongly affected not only by its shape [7, 11]
58 but also by hydrogen absorption characteristics of the hydrogen storage alloy used. Honjo
59 et al. [4] and Nakai et al. [5] investigated deformation of unimorph actuators using La-Ni
60 and Pd-Ni alloys, respectively, and showed their displacement amounts and response rates
61 were dependent on the composition of alloys. It is also important to investigate the
62 swelling ability during hydrogen absorption in a hydrogen storage alloy itself. Some
63 studies have been performed using powder as a sample, in which various measurement
64 methods were adopted, for example, optically [14, 15], electrically [16, 17], and with
65 strain gauges on a sample holder [18-20].
66 A hydrogen absorption behavior of a hydrogen storage alloy is also affected by stress.
67 Hydrogen content thermodynamically decreases with increasing compressive stress, and
68 vice versa [21, 22]. The diffusion is promoted not only by a hydrogen content gradient

(Fick's law) but also by a stress gradient [23, 24]. Many researchers [25-28] simulated diffusion of hydrogen atoms in a hydrogen storage alloy under stress, which revealed that the so-called stress-induced diffusion (SID) plays an important role in the diffusion behavior. In the actuator, the stress effect cannot be negligible because it receives a reaction force during operation.

In this paper, the response behavior of the capsule-type HSA actuator was investigated. Displacement of an actuator made of palladium and epoxy resin was measured with changing H_2 pressure. To reveal its internal state, a numerical simulation was performed and compared with the experimental results.

2. Experiment

The fabricated sample of the capsule-type HSA actuator is shown in Figure 2. It was almost spherical with outer diameter of 22.1 ± 0.4 mm on the equator (Figure 2a-c). From a cross-sectional observation after the experiment (Figure 2d), the sample was confirmed to have a hollow cylindrical structure with inner diameter of ~13.2 mm. Its design dimensions are shown in Figure 2e.

It was fabricated as follows (Figure 3). Palladium foil with 0.08 mm in thickness and epoxy resin were used as the HSA foil and capsule, respectively. The foil (Tanaka Kikinzoku Kogyo K.K.) of 15 x 42 x 0.08 mm was annealed in the air at 400^{o}C for 2 hours (1 & 2) to remove the residual stress induced by rolling. The annealed foil was looped on a core made of wax, which is used to make the sample hollow (3). The epoxy resin was prepared by mixing Epon828 (Polyscience, Inc.) with diethylenetriamine (Alfa Aesar) (4), followed by vacuum degassing for 5 min (5). It was cast between a silicone mold and the core with the foil (6). After solidified for 24 hours at room temperature, it

92 was heated at 80^{o}C in the air to remove the core (7). The sample was finally cleaned with
93 2-propanol. Although the palladium foil formed an oxide layer during the annealing
94 (Figure 2a), it was cleaned after hydrogen charge, and its color recovered to silver (Figure
95 2c). No delamination between the HSA foil and the capsule was observed after the
96 experiments (Figure 2d).
97 The sample was fixed perpendicular to the ground in a pressure vessel. Then, a piston
98 was put on the sample. Displacement of the piston i.e. height change of the sample u was
99 measured with a laser displacement sensor (LK-G85, Keyence) through a viewing
100 window of the pressure vessel at room temperature. The measurement apparatus is
101 described in detail in [14]. The purity of hydrogen gas (Taiyo Nippon Sanyo Co.) was
102 99.999% or more. Before the measurement, hydrogen was introduced into the evacuated
103 vessel at 5 atm for $3x10^4$ s, followed by the evacuation, for an activation treatment.
104 The hydrogen pressure was rapidly changed by opening a valve connected to a
105 hydrogen tank or a rotary vacuum pump at t = 0 s, and then, the vessel was kept at the
106 constant pressure to measure the response time. It is noted that hydrogen was charged not
107 only in the capsule but inside the whole of the pressure vessel. The measurement interval
108 was 0.1 or 1 s during the pressurization and 1 s during the evacuation.

109 **3. Experimental results**

110 Figure 4 shows the displacement change in time during the pressurization and the
111 following evacuation at the introduced hydrogen pressure P_{intro} of 4.90 atm. The
112 displacement u_i at t = 0 s was set to 0.0 μm. The positive value represents an increase in
113 the capsule height. During the pressurization (Figure 4a), hydrogen pressure yielded 90%
114 of P_{intro} within 6 s. At the same time, the displacement increased by 7.5 μm (= u_P) in

proportion to the pressure. The displacement continued increasing after the pressure change, and it yielded a maximum value u_{max} of 10.0 μm at t = 245 s, followed by decreasing. The final displacement u_f was -6.5±0.2 μm, where the error range represents the standard deviation calculated from the values at last 100 s.

The first increase in the displacement at the same time as the pressurization u_P was caused by the changes in a refractive index in the vessel and shrinkage of the capsule due to hydrostatic pressure. The refractive index depends on gas species and its pressure and temperature. Its contribution is estimated at 1.0 μm/atm from Snell's law. The displacement by the hydrostatic pressure was estimated at -0.2 μm/atm by a finite element analysis. The total contribution of the refractive index and hydrostatic pressure is, therefore, 0.8 μm/atm, which roughly agrees with u_P. The refractive index change does not affect the deformation in the practical environment, because hydrogen is charged only in the capsule. The following increase in displacement is caused by thermal expansion. The enthalpies of hydrogen absorption in solid solution and the phase transition into hydride are -4620 and -9440 cal/molH_2, respectively in palladium [29], indicating both reactions are exothermal reactions. Therefore, the temperature in the HSA foil increases during the pressurization. A net actuator's displacement U is calculated as $|u_f - u_P|$, i.e., 14.0 μm.

During the evacuation (Figure 4b), the displacement almost recovered to 0. It decreased by 7.5 μm soon after the evacuation (u_P). It is due to the change in hydrostatic pressure and refractive index as well as during the pressurization. Under the constant pressure of 0.00 atm, the displacement gradually increased. The final displacement u_f was 1.3±0.2 μm. The net displacement U was calculated as 15.0 μm, which is comparable to that during the pressurization. The difference of U between during the pressurization and

evacuation is considered to involve the effects of the plastic deformation of the capsule. The similar tendencies were obtained at other P_{intro}. All data are tabulated in Table 1.

Table 1 Displacement values at each P_{intro}.

	Pressurization						Evacuation				
P_{intro} [atm]	u_i [μm]	u_P [μm]	u_{max} [μm]	u_f [μm]	U [μm]	t_{80} [s]	u_i [μm]	u_P [μm]	u_f [μm]	U [μm]	t_{80} [s]
1.16	0.0	0.8	2.9	-4.1	4.9	3348	-4.9	-2.0	-1.0	5.9	2358
1.97	0.0	2.2	4.7	-4.7	6.9	4936	-12.1	-2.8	-6.3	8.6	4045
2.88	0.0	5.4	6.6	-7.5	12.9	1966	-7.9	-4.3	-1.8	10.4	2333
2.91	0.0	5.8	6.6	-4.3	10.1	3055	-5.7	-5.0	-1.7	9.1	4071
4.89	0.0	7.9	10.3	-7.3	15.2	1911	-7.9	-7.1	-1.4	13.7	3370
4.90	0.0	7.5	10.0	-6.5	14.0	1521	-6.2	-7.5	1.3	15.0	2183

Figure 5 shows a variation of the net displacement U with P_{intro}. U during the evacuation was comparable to that during the pressurization at all P_{intro}, indicating that the actuator reversibly deformed. Larger net displacement was obtained at higher pressure, and its increment decreased with the pressure increase.

The dependence of response time on pressure was different during the pressurization and evacuation as shown in Figure 6. The 80% response time t_{80} represents a time to yield 80% of the net displacement. During the pressurization (Figure 6a), t_{80} decreased with P_{intro}. The response time at P_{intro} < 2 atm was half of that at P_{intro} = 5 atm. During the evacuation (Figure 6b), t_{80} was independent of P_{intro} although the large scatter was

observed. The similar scattering was also observed in our previous measurement using the same measurement system [14]. The evacuation pressure and purity of the gas in the pressure chamber depend on the ambient temperature and humidity, leak property of the chamber and performance of the vacuum pump. The scattering will become small if the evacuation system is improved.

4. Numerical simulation of HSA actuator's response

The diffusion-mechanical coupling analysis revealed an internal state of the actuator. In the simulation, hydrogen diffusion was driven not only by concentration gradient but also by stress gradient. Most of the papers relevant to the stress-induced diffusion [21-28] focus on hydrogen embrittlement in steel and hydrogen permeable membranes, in which hydrogen content is small enough to neglect the effect of volume and activity change with hydrogen content. In the actuator's applications, these effects should be taken into account since the hydrogen content can be high. The diffusion equation used in this work is as follows.

$$J = -D''\nabla n_H + \frac{D' n_H V_H}{RT}\nabla \sigma_h \quad (1)$$

where J: flux of hydrogen, D' and D'': modified hydrogen diffusion coefficients, n_H: molar ratio of hydrogen to metal (H/M), V_H: partial molar volume of hydrogen, R: universal gas constant, T: temperature, and σ_h: hydrostatic stress. The derivation of Eq. (1) is shown in Appendix A. Goto et al. [28] showed that the stress gradient does not significantly contribute to the diffusion behavior compared to the activity change with hydrogen content, while the equilibrium hydrogen content is affected by the stress. A surface flux of the HSA foil was calculated from a difference between chemical potentials of hydrogen gas and atoms at the surface. The detailed analytical condition is shown in

Appendix B. The displacement amount under 1 atm of hydrogen was 6.9 μm (Figure B.2), which almost agreed with the experimental result (4.9 μm at 1.16 atm). The difference between the experiment and simulation seemingly comes from local stress relaxation and incompleteness of the sample shape. The stress is locally reduced at corners of the HSA foil due to plastic and viscoelastic deformation in the epoxy resin, which decreases the displacement. The plasticity and viscoelasticity in the capsule were not taken into account in the present simulation. Also, the capsule shape of the sample is not completely spherical. Investigation of these effects on the displacement is the future task.

The simulation revealed the internal state of the actuator. Figure 7 shows the time change of hydrogen content n_H and compressive hydrostatic stress σ_h in the HSA foil when a deformation ratio was 1.3, 14.9, 83.4 and 100%, respectively. The deformation ratio was calculated by dividing displacement by final displacement. The transverse axis represents the thickness of the foil in the radial direction on the equator position. n_H gradually increased with time near the surface and diffused into the inside. The foil was subjected to the higher compressive stress with the increase in the hydrogen content because its surrounding capsule resisted the deformation. n_H and σ_h at t = 3000 s were 5.4×10^{-3} and 22.3 MPa, respectively. σ_h at the boundaries was lower than inside because the stress in the radial direction becomes nearly 0 on the boundaries.

5. Discussions

The simulation indicates that hydride is not formed in the HSA foil during the deformation. Under free stress, the phase transition pressure between solid solution and hydride in palladium is 1×10^{-2} atm [30]. Therefore, at 1 atm, the hydride is not formed in palladium, and its equilibrium hydrogen content is n_H = 0.72 [31]. However, n_H = 0.0054

199 in the simulation, which is more than 100 times smaller than 0.72. The palladium-
200 hydrogen system forms solid-solution state at $n_H < 0.03$. This is why the deformation in
201 the experiment was much less than that expected with the technique used in [11]. The low
202 equilibrium hydrogen content is due to the high compressive stress.
203 The response time decreased with the increase in the introduced hydrogen pressure
204 P_{intro} during the pressurization, while it is independent during the evacuation. The same
205 tendency was observed when hydrogen was charged into palladium powder [14]. The
206 driving force of hydrogen absorption/discharge increases with the pressure difference
207 between applied pressure P_{ap} and equilibrium pressure P_{eq} [32], where $P_{ap} = P_{intro}$ during
208 the pressurization and $P_{ap} = 0$ atm during the evacuation. The constant response time
209 independent of the pressure at the time of evacuation implies the existence of the rate-
210 determining step which gives constant P_{eq} such as interfacial reaction.
211 It took a few thousand seconds during both of the pressurization and evacuation to
212 complete the deformation. In contrast, when the volume change of palladium powder was
213 measured under free stress [14], the response time during the evacuation was longer than
214 that during the pressurization. The difference comes from the phase of palladium-
215 hydrogen system: solid solution in the actuator, while hydride under free stress. Ulvestad
216 et al. [33] pointed out that a hydride on palladium surface decreases a hydrogen discharge
217 rate. In this study, the simulation indicates the hydride was not formed during the
218 deformation due to the compressive stress, hence, the response time during the evacuation
219 was similar during the pressurization.
220 The temperature also affects the response time of the actuator. The reaction rate
221 increases with temperature. During the pressurization, the response time can be increased
222 by the exothermal reaction of absorption. The evaluation of the thermal effect is the future

task.

6. Conclusion

In this paper, a capsule-type hydrogen-storage-alloy (HSA) actuator made of palladium and epoxy resin as an HSA foil and a capsule was fabricated, and its response behavior in hydrogen was investigated. Moreover, a mechanical finite element analysis coupled with diffusion problem was performed to investigate its internal state. The main conclusions are summarized as follows;

1. The displacement was observed when hydrogen gas was charged. By the following evacuation, it recovered to almost 0.
2. Larger displacement was obtained at higher pressure, and its increment decreased with the pressure increase.
3. The displacement rate increased with H_2 pressure during the pressurization, while it was independent of the pressure during the evacuation.
4. The solid solution phase is formed inside the palladium foil during deformation due to compressive stress.

Thus, the response behavior of the capsule-type HSA actuator is strongly affected by the stress, especially in terms of the absorbed hydrogen amount. The performance of the actuators can be improved by designing to decrease stress in the hydrogen storage alloy.

Although the epoxy resin was used for the capsule in this work due to easy forming, it is not suitable in practical use since hydrogen penetrates the resin. The candidate materials for the capsule are an aluminum alloy and stainless steel, which has high resistance to hydrogen penetration. It is a future task to develop the fabrication process of the capsule-type actuator with these materials. However, the knowledge obtained in this work is

246 useful for the design of all HSA actuators.

247 **Appendix A. Derivation of diffusion equation**

248 Chemical potential, μ_H including a stress term is represented as Eq. (A.1).

249 $$\mu_H = \mu_H^0 + RT \ln a_H - V_H \sigma_h \quad \text{(A. 1)}$$

250 where a_H is the activity of hydrogen. a_H is represented with the hydrogen content n_H and
251 the activity coefficient γ_n as $a_H = \gamma_n n_H$. Hydrogen flux in a hydrogen storage alloy J is
252 proportional to a chemical potential gradient.

253 $$J = -\alpha \nabla \mu_H = -\alpha \left\{ \frac{RT}{n_H} \left(1 + \frac{\partial \ln \gamma_H}{\partial \ln n_H} \right) \nabla n_H - V_H \nabla \sigma_h \right\} \quad \text{(A. 2)}$$

254 In case of $n_H << 1$ and free stress, Eq. (A.2) corresponds to Fick's equation.

255 $$J = -\alpha \frac{RT}{n_H} \nabla n_H = -D \nabla C_H \quad \text{(A. 3)}$$

256 $$\therefore \alpha = \frac{D n_H}{RT} \frac{dC_H}{dn_H} \quad \text{(A. 4)}$$

257 where C_H is the molar concentration and D is Fick's diffusion coefficient. A lattice volume
258 of palladium increases in proportion to n_H at $n_H < 0.75$ [34]. The relationship between C_H
259 and n_H, therefore, is represented as Eq. (A.5) using V_H and molar volume of palladium
260 V_M.

261 $$C_H = \frac{n_H}{V_M + n_H V_H} \quad \text{(A. 5)}$$

262 From Eqs. (A.2), (A.4) and (A.5),

263 $$J = -D \frac{V_M}{(V_M + n_H V_H)^2} \left(1 + \frac{\partial \ln \gamma_H}{\partial \ln n_H} \right) \nabla n_H + \frac{D n_H V_H}{RT} \frac{V_M}{(V_M + n_H V_H)^2} \nabla \sigma_h \quad \text{(A. 6)}$$

264 Eq. (1) is derived by defining *D'* and *D''* as

265 $$D' = D \frac{V_M}{(V_M + n_H V_H)^2}, D'' = D' \left(1 + \frac{\partial \ln \gamma_H}{\partial \ln n_H} \right) \quad \text{(A. 7)}$$

266 *D'* includes the effect of the volume change during absorption, and *D''* reflects the change

in the activity in addition to the volume change.

The activity coefficient was determined from a PCT diagram of the palladium-hydrogen system [31]. The chemical potential of molecules in the gas μ_{H2} is same as that of atoms in the alloy in the equilibrium condition, i.e.,

$$\mu_H = \frac{1}{2}\mu_{H2} = \frac{1}{2}\left(\mu_{H2,0} + RT \ln f_{H2}\right) \quad \text{(A. 8)}$$

where f_{H2} is the fugacity. From Eqs. (A.1) and (A.8),

$$\gamma_H = \frac{(f_{H2})^{\frac{1}{2}}}{n_H} \exp\left\{\frac{1}{RT}\left(\frac{1}{2}\mu_{H2,0} - \mu_H^0\right)\right\} \quad \text{(A. 9)}$$

where it is noted that the stress gradient $\nabla\sigma_h$ is 0 in the PCT measurement. Therefore,

$$\frac{\partial \ln \gamma_H}{\partial \ln n_H} = \frac{n_H}{\gamma_H}\frac{\partial \gamma_H}{\partial n_H} = \frac{n_H}{2f_{H2}}\frac{\partial f_{H2}}{\partial n_H} - 1 \quad \text{(A. 10)}$$

By substituting Eq. (A.10) into Eq. (A.7), Eq. (A.11) is obtained.

$$D'' = D'\left(\frac{n_H}{2f_{H2}}\frac{\partial f_{H2}}{\partial n_H}\right) \quad \text{(A. 11)}$$

$f_{H2} = P_{H2}$ at a few atm where the HSA actuator is used. The relationship between n_H and P_{H2} is obtained from the PCT diagram [31].

Figure A.1 shows the variations of *D'* and *D"* with n_H at $n_H < 0.03$ used in the present work, assuming $D = 3.75\text{x}10^{-11}$ m^2/s [35], $V_H = 1.73$ cm^3/mol [34], and $V_M = 8.864$ cm^3/mol [37].

Appendix B. Simulation method

To simulate the deformation of the actuator with hydrogen diffusion, a diffusion-mechanical coupled analysis was performed using the finite element method. Governing equations used were Eq. (1) and Eq. (B.1) in the diffusion and mechanical analysis, respectively.

$$\boldsymbol{\sigma} = \boldsymbol{c\varepsilon} + \boldsymbol{\beta} n_H \quad \text{(B. 1)}$$

where $\boldsymbol{c}$ is the stiffness tensor given by Young's modulus E and Poisson's ratio ν, $\boldsymbol{\beta}$ is a tensor in which diagonal components are the linear expansion ratio, b induced by hydrogen insertion and non-diagonal components have zero values. The calculation procedure is shown in [28].

An analytical model was a 2D axisymmetric model of the capsule-type HSA actuator (Figure B1a), where we ignored the difference in shape between Figure 1 and the experimental sample (Figure 2). It consists of parts representing an HSA foil, a capsule, and an HSA surface layer. In the diffusion analysis, the hydrogen content in the capsule part was kept 0 to assume the diffusion only in the foil. The model was meshed with a four-node quadrilateral element as shown in Figure B1b. The HSA foil part was meshed in 10 layers. The total number of nodes was 14564. The evaluation was performed at each integration point using the commercial FEM software package ANSYS 17.0. The material parameters used are shown in Table B.1. The linear expansion ratio b was calculated from the volume expansion ratio, i.e., $b = V_H/3V_M$. A time step was 1 s for the transient diffusion analysis.

Table B.1 Material properties used in analysis.

	E [GPa]	ν [-]	V_H [cm^3/mol]	V_M [cm^3/mol]	b [-]
Palladium	121 [36]	0.39 [36]	1.73 [34]	8.864 [37]	0.0652
Epoxy resin [38]	3.80	0.25	-	-	-

The distribution of n_H obtained from the diffusion analysis was input as a boundary condition in the mechanical analysis, and symmetrical boundary conditions were applied

309 on x = y = 0.

310 In the diffusion analysis, the stress distribution obtained from the mechanical analysis
311 at the previous iteration was applied to each node. n_H at the surface layer part was
312 determined as follows. Based on the reaction H_2 (g) ⇔ H+H (solid solution), assume that
313 rates of inflow $J_{H2,in}$ and outflow $J_{H,out}$ on the foil surface are in proportion to the pressure
314 and the square of the activity under free stress $a_{H,0}$, respectively. The surface flux of
315 hydrogen atoms J_S is represented as

316 $$J_S = 2J_{H2,in} - J_{H,out} = 2k_{in}P_{H2} - k_{out}{a_{H,0}}^2 \quad \text{(B. 2)}$$

317 where k_{in} and k_{out} are constants. At the equilibrium condition, $\mu_{H2} = 2\mu_H$ and $J_S = 0$.
318 Therefore,

319 $$J_S = K_t\left(P_{H2} - P_{H2}^0{K_S}^2{a_{H,0}}^2\right) \quad \text{(B. 3)}$$

320 where $K_t = 2k_{in}$. The activity a_H changes under stress, i.e.,

321 $$a_H = a_{H,0}\exp\left(\frac{V_H\sigma_h}{RT}\right) \quad \text{(B. 4)}$$

322 By substituting Eq. (B.4), Eq. (B.3) becomes

323 $$J_S = K_t\left\{P_{H2} - P_{H2}^0{K_S}^2{a_H}^2\exp\left(-\frac{2V_H\sigma_h}{RT}\right)\right\} \quad \text{(B. 5)}$$

324 The hydrogen content at the surface boundary layer at time t+1 is represented as Eq. (B.6).

325 $$n_H(t+1) = n_H(t) + \frac{K_tA_S}{V_S}\left\{P_{H2} - P_{H2}^0{K_S}^2{a_H}^2\exp\left(-\frac{2V_H\sigma_h}{RT}\right)\right\}\Delta t \quad \text{(B. 6)}$$

326 where A_S is the surface area, V_S is the volume of the layer and δt is the time step. In this
327 work, P_{H2} and K_t were set as 1 atm and $1\text{x}10^{-4}$ mm/atm/s, respectively.

328 Figure B.2 shows a variation of the displacement U_{FEM} with time obtained from the
329 numerical simulation, assuming that hydrogen of 1 atm was charged at t = 0 s. U_{FEM}
330 decreased, i.e. the capsule shrank in the height direction, with the increase in time. u_{max}
331 was not shown because the effect of thermal expansion was ignored. The deformation

was completed after 3000 s, and the final displacement was -6.9 μm. The response time was shorter than the experimental result. We assumed K_t = 1x10^{-4} mm/atm/s, which is not a measured value and sensitive to the surface condition. This is why the deformation rate was different in the simulation and experiment. However, the difference is not discussed in this paper because the response time does not affect the internal state qualitatively.

Acknowledge

This work was financially supported by JSPS KAKENHI Grant Number JP15J00233 and JP16K05969.

Reference

[1] T.I. Sigfusson, Hydrogen island: the story and motivations behinds the Icelandic hydrogen society experiment, Mitig. Adapt. Strat. Glob. Change 12 (2007) 407-418. https://doi.org/10.1007/s11027-006-9075-0

[2] N. Behling, M.C. Williams, S. Managi, Fuel cells and the hydrogen revolution: Analysis of a strategic plan in Japan, Econ. Anal. Pol. 48 (2015) 204-221. https://doi.org/10.1016/j.eap.2015.10.002

[3] Y. Nishi, H. Uchida, T. Honjo, High responsiveness induced by palladium deposition on thin film actuator of $LaNi_5$ hydrogen storage alloy, Mater. Trans. 46 (2005) 126-129. https://doi.org/10.2320/matertrans.46.126

[4] T. Honjo, H. Yabe, S. Tsubuteishi, H. Uchida, Y. Nishi, Chemical composition dependence of the Properties of a $LaNi_x$ (x = 3.8 to 6.5) hydrogen storage alloy film actuator, J. Jpn. Inst. Met. Mater. 67 (2003) 145-148. https://doi.org/10.2320/jinstmet1952.67.4_145

[5] A. Nakai, M. Mizumoto, A. Kagawa, Bending and rotation movement control of a

355 novel actuator utilizing hydrogen storage alloys, Adv. Mater. Res. 156-157 (2011) 1170-
356 1175. https://doi.org/10.4028/www.scientific.net/AMR.156-157.1170
357 [6] M. Mizumoto, T. Ohgai, A. Kagawa, Bending behavior of Cu-plated Pd-Ni alloys
358 ribbon driven by hydrogenation, J. Alloy. Comp. 482 (2009) 416-419.
359 https://doi.org/10.1016/j.jallcom.2009.04.041
360 [7] A. Kagawa, K. Taniguchi, M. Yamamoto, Designs for miniaturization of bending
361 actuator utilizing hydrogen storage alloy, J. Alloy. Comp. 563 (2013) 203-206.
362 https://doi.org/10.1016/j.jallcom.2013.02.088
363 [8] K. Yuse, D. Guyomar, M. Kanda, L Seveyrat, B. Guiffard, Development of large-
364 strain and low-powered electro-active polymers (EAPs) using conductive fillers, Sens.
365 Actuators A 165 (2011) 147-154. https://doi.org/10.1016/j.sna.2010.08.008
366 [9] Y. Nishi, J. Ohkawa, M.C. Faudree, M. Kanda, K. Yuse, D. Guyomar, H. Uchida, An
367 improved H_2-gas pressure operated $LaNi_5$ powder-dispersed polyurethane/titanium 2-
368 layer actuator with reversible giant and rapid expansion by hydrogenation, Mater. Trans.
369 59 (2018) 129-135. https://doi.org/10.2320/matertrans.M2017212
370 [10] M. Mizumoto, T. Ohgai, A. Kagawa, Development of actuator utilizing hydrogen
371 storage alloys, in: T. Higuchi, K. Suzumori, S. Tadokoro (Eds.), Next-Generation
372 Actuators Leading Breakthroughs, Springer-Verlag, London, 2010, pp. 337-349.
373 https://doi.org/10.1007/978-1-84882-991-6
374 [11] K. Goto, T. Higuchi, O. Fuchiwaki, W. Nakao, Design of capsule-type micro actuator
375 utilizing hydrogen storage alloys by finite element analysis, Trans. Mater. Res. Soc. Jpn.
376 39 (2014) 145-152. https://doi.org/10.14723/tmrsj.39.145
377 [12] K. Goto, T. Higuchi, O. Fuchiwaki, W. Nakao, Deformation behavior of capsule-
378 type micro actuator using palladium, Proc. ASME 2015 Conf. Smart Mater. Adapt. Struct.

379 Intell. Syst. 1 (2015) V001T01A017. https://doi.org/10.1115/SMASIS2015-9034
380 [13] S. Kuroda, T. Higuchi, Y. Tsujimoto, S. Ueno, The relative speed control of super
381 multi-link space manipulator to capture space debris, SICE J. Control Meas. Syst. Integr.
382 10 (2017) 229-236. https://doi.org/10.9746/jcmsi.10.229
383 [14] K. Goto, T. Hirata, I. Yamamoto, W. Nakao, Swelling response behavior of palladium
384 during hydrogen absorption and discharge, Int. J. Hydrogen Energy 43 (2018) 11092-
385 11099. https://doi.org/10.1016/j.ijhydene.2018.04.199
386 [15] M. Matsushita, M. Monde, Y. Mitsutake, Experimental formula for estimating
387 porosity in a metal hydride packed bed, Int. J. Hydrogen Energy 38 (2013) 7056-7064.
388 https://doi.org/10.1016/j.ijhydene.2013.04.005
389 [16] E.S. Ribeiro, J.M. Gil, A novel capacitive device for the study of volumetric
390 expansion of hydride powders, Int. J. Hydrogen Energy 40 (2015) 14900-14910.
391 https://doi.org/10.1016/j.ijhydene.2015.08.063
392 [17] B. Charlas, A. Chaise, O. Gillia, P. Doremus, D. Imbault, Investigation of hydride
393 powder bed swelling and shrinking during hydrogen absorption/desorption cycles under
394 different compressive stresses, J. Alloy. Comp. 580 (2013) S149-152.
395 https://doi.org/10.1016/j.jallcom.2013.01.192
396 [18] K. Nasako, Y. Ito, N. Hiro, M. Osumi, Stress on a reaction vessel by the swelling of
397 a hydrogen absorbing alloy, J. Alloy. Comp. 264 (1998) 271-276.
398 https://doi.org/10.1016/S0925-8388(97)00246-6
399 [19] T. Saito, K. Suwa, T. Kawamura, Influence of expansion of metal hydride during
400 hydriding-dehydriding cycles, J. Alloy. Comp. 253-254 (1997) 682-685.
401 https://doi.org/10.1016/S0925-8388(96)02893-9
402 [20] C. Lin, S. Huang, Y. Jhang, Effects of cyclic hydriding-dehydriding reactions of

403 Mg_2Ni alloy on the expansion deformation of a metal hydride storage vessel, J. Alloy.
404 Comp. 509 (2011) 7162-7167. https://doi.org/10.1016/j.jallcom.2011.04.038
405 [21] J.O'M. Bockris, W. Beck, M.A. Genshaw, P.K. Subramanyan, F.S. Williams, The
406 effect of stress on the chemical potential of hydrogen in iron and steel, Acta Metall. 19
407 (1971) 1209-1218. https://doi.org/10.1016/0001-6160(71)90054-X
408 [22] H.A. Wriedt, R.A. Oriani, Effect of tensile and compressive elastic stress on
409 equilibrium hydrogen solubility in a solid, Acta Metall. 18 (1970) 753-760.
410 https://doi.org/10.1016/0001-6160(70)90039-8
411 [23] B. Baranowski, Stress-induced diffusion in hydrogen permeation through $Pd_{81}Pt_{19}$
412 membranes, J Less Common Met. 154 (1989) 329-353. https://doi.org/10.1016/0022-
413 5088(89)90218-X
414 [24] K. Kandasamy, Influences of self-induced stress on permeation flux and space-time
415 variation of concentration during diffusion of hydrogen in a palladium alloy, Int. J.
416 Hydrogen Energy 20 (1995) 455-463. https://doi.org/10.1016/0360-3199(94)00074-A
417 [25] W.S. Zhang, M.Q. Hou, H.Y. Wang, Y.B. Fu, Numerical simulation of diffusivity of
418 hydrogen in thin tubular metallic membranes affected by self-stresses, Int. J. Hydrogen
419 Energy 29 (2004) 1165-1172. https://doi.org/10.1016/j.ijhydene.2003.10.007
420 [26] A. Adrover, M. Giona, L. Capobianco, V. Violante, Effects of self-stress on hydrogen
421 diffusion in Pd membranes in the coexistence of α and β phases, J. Alloy. Comp. 368
422 (2004) 287-297. https://doi.org/10.1016/j.jallcom.2003.06.003
423 [27] W.S. Zhang, Z.L. Zhang, X.W. Zhang, Effects of self-stress on the hydrogen
424 absorption into palladium hydride electrodes of plate form under galvanostatic conditions,
425 J. Electroanal. Chem. 474 (1999) 130-137. https://doi.org/10.1016/S0022-
426 0728(99)00318-6

427 [28] K. Goto, S. Ozaki, W. Nakao, Effect of diffusion coefficient variation on interrelation
428 between hydrogen diffusion and induced internal stress in hydrogen storage alloys, J.
429 Alloy. Comp. 691 (2017) 705-712. https://doi.org/10.1016/j.jallcom.2016.08.288
430 [29] E. Wicke, H. Brodowski, H. Züchner, Hydrogen in palladium and palladium alloys.
431 In: G. Alefeld, J. Völkl editors. Hydrogen in Metals II, Berlin: Springer; 1978, p. 73-155.
432 [30] T.B. Flanagan, W. Luo, J.D. Clewley, Calorimetric enthalpies of absorption and
433 desorption of protium and deuterium by palladium, J. Less Common Met. 172-174 (1991)
434 42-55. https://doi.org/10.1016/0022-5088(91)90431-3
435 [31] B. Baranowski, F.A. Lewis, W.D. McFall, S. Filipek, T.C. Witherspoon, A study of
436 the palladium-platinum-hydrogen system over a wide range of hydrogen pressures, Proc.
437 Royal Soc. A 386 (1983) 309-332. https://doi.org/10.1098/rspa.1983.0038
438 [32] C.N. Park, J.Y. Lee, Kinetic properties of the hydrogenation of the FeTi intermetallic
439 compound, J. Less Common Met. 91 (1983) 189-201. https://doi.org/10.1016/0022-
440 5088(91)90431-3. https://doi.org/10.1016/0022-5088(83)90312-0
441 [33] A. Ulvestad, M.J. Welland, S.S.E. Collins, R. Harder, E. Maxey, J. Wingert, A. Singer,
442 S. Hy, P. Mulvaney, P. Zapol, O.G. Shpyrko, Avalanching strain dynamics during the
443 hydriding phase transformation in individual palladium nanoparticles, Nat. Commun. 6
444 (2015) 10092. https://doi.org/10.1038/ncomms10092
445 [34] B. Baranowski, S. Majchrzak, T.B. Flanagan, The volume increase of fcc metals and
446 alloys due to interstitial hydrogen over a wide range of hydrogen contents, J. Phys. F Met.
447 Phys. 1 (1971) 258-261. https://doi.org/10.1088/0305-4608/1/3/307
448 [35] Y. Fukai, H. Sugimoto, Diffusion of hydrogen in metals, Adv. Phys. 34 (1985) 263-
449 326. https://doi.org/10.1080/00018738500101751
450 [36] Z. Sauli, V. Retnasamy, S. Taniselass, W.M.W. Norhaimi, M.H.A. Aziz, M.N.

Hashim, Effect of copper FAB impact on palladium bond pad, Proc. 2012 10th IEEE Int. Conf. Semicond. Electron. (2012) 316-319. https://doi.org/10.1109/SMElec.2012.6417149

[37] Y. Sakamoto, X.Q. Tong, F.A. Lewis, Effects of non-fickian uphill components of permeation flux on estimations of hydrogen diffusion coefficients in the Pd/H system, Scr. Metall. Mater. 25 (1991) 1629-1634. https://doi.org/10.1016/0956-716X(91)90465-D

[38] K.C. Radford, The mechanical properties of an epoxy resin with a second phase dispersion, J. Mater. Sci. 6 (1971) 1286-1291. https://doi.org/10.1007/BF00552042

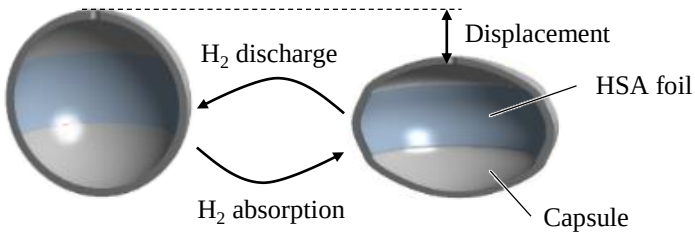

Figure 1 Schematics of capsule-type hydrogen-storage-alloy (HSA) actuator and its deformation.

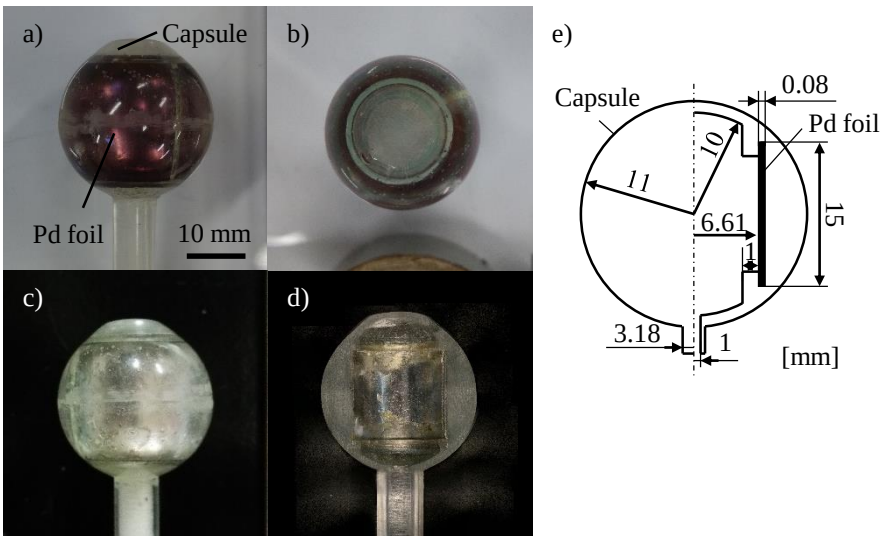

Figure 2 Sample : a) side and b) top view of outer surface after fabrication, c) outer surface and d) cross section after experiment, and e) schematic image with design dimensions.

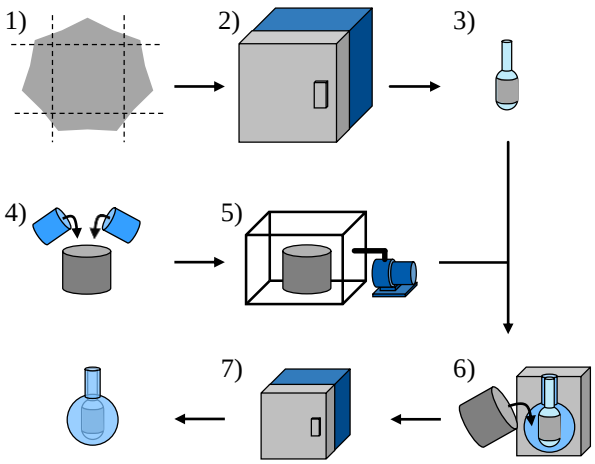

Figure 3 Fabrication procedure of capsule-type HSA actuator: 1) cutting HSA foil, 2) annealing HSA foil, 3) winding HSA foil around core, 4) mixing Epon 828 and DETA, 5) vacuum degassing, 6) injection epoxy resin into mold with core, and 7) discharge of core by melting.

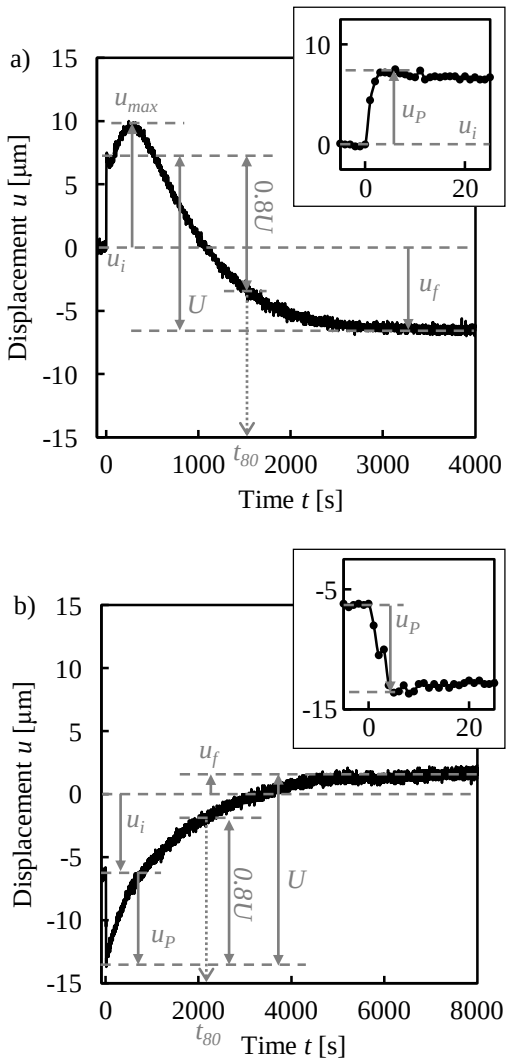

Figure 4 Time change of displacement a) during pressurization and b) at following evacuation at P_{intro} of 4.903 atm.

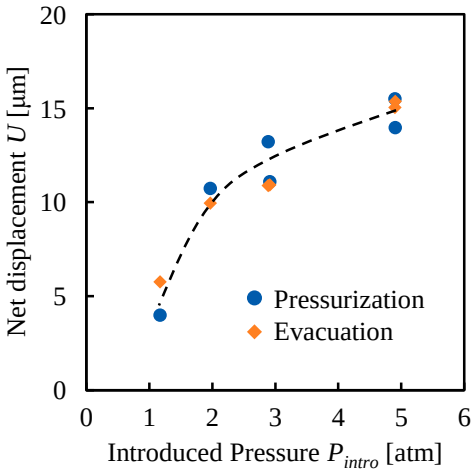

Figure 5 Dependence of net displacement on introduced H_2 pressure.

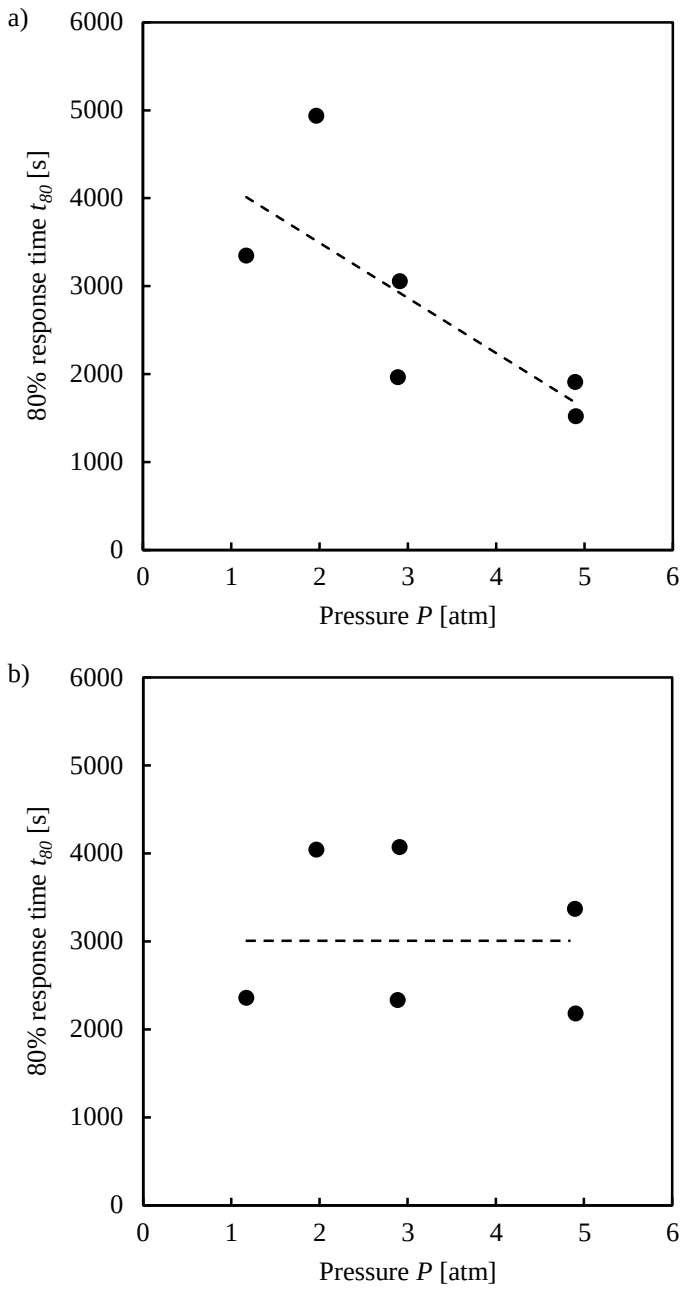

Figure 6 Dependence of response time when deformation ratio reached 80% on pressure at a) H_2 introduction and b) evacuation

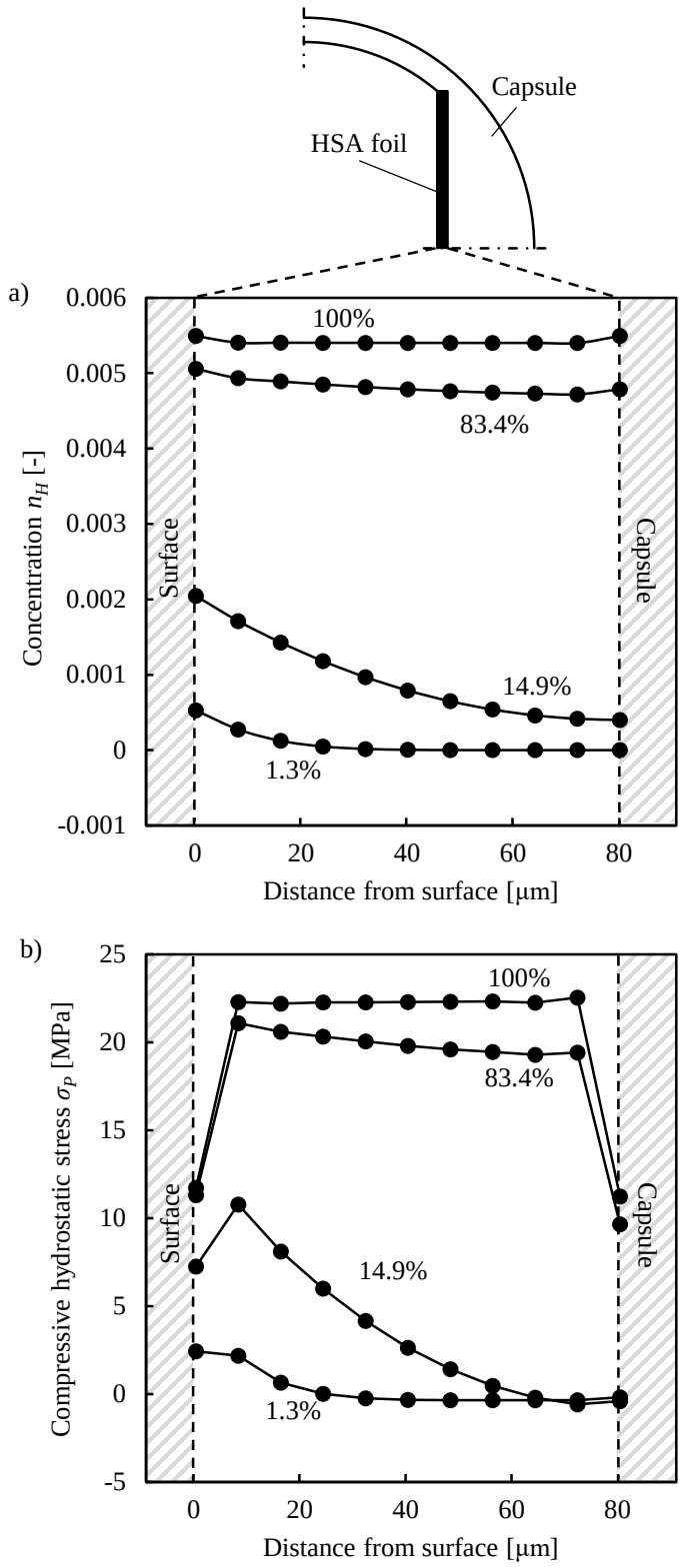

Figure 7 Distribution of a) hydrogen content and b) compressive hydrostatic stress in hydrogen-storage-alloy foil at various deformation ratio. The deformation ratio was calculated by divided by the final displacement.

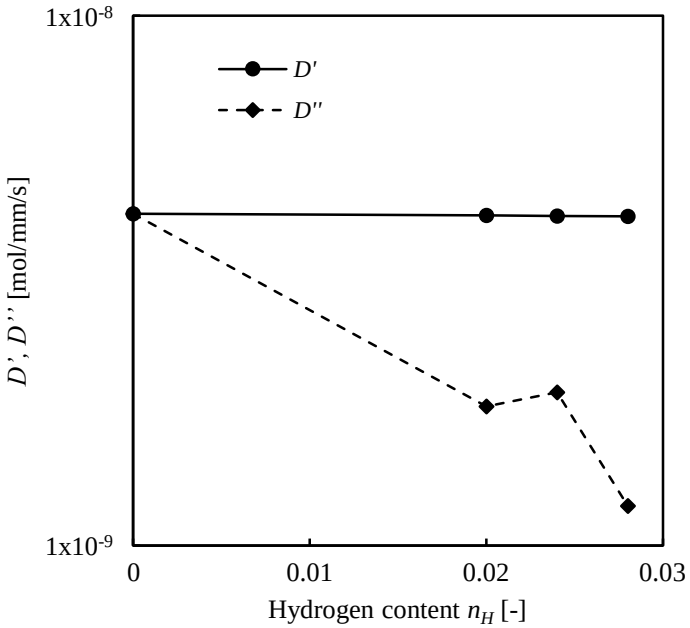

Figure A.1 Variation of modified diffusion coefficients *D'* and *D''* with hydrogen content.

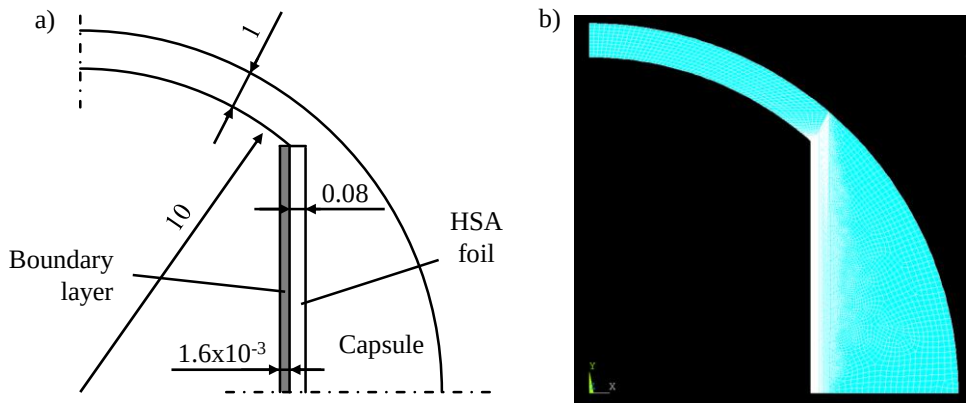

Figure B.1 a) Schematic of analytical model and b) finite element model for diffusion-structural coupling analysis of capsule-type HSA actuator.

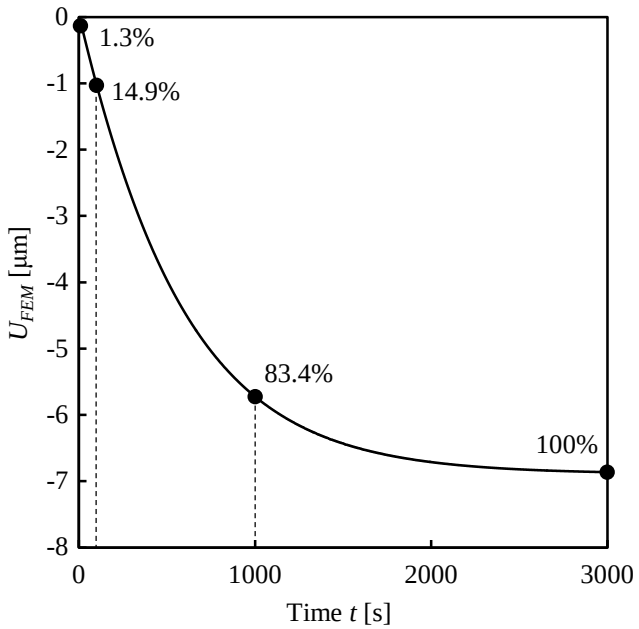

Figure B.2 Displacement change with time at P_{intro} = 1 atm in numerical simulation. It corresponds to doubled displacement at the top of the analytical model. The value at each plot represents the deformation ratio.